Effect of Loop Orientation on Quadruplex−TMPyP4 Interaction

Amit Arora and Souvik Maiti*

Proteomics and Structural Biology Unit, Institute of Genomics and Integrative Biology, CSIR, Mall Road, Delhi 110 007, India

Received: December 10, 2007; Revised Manuscript Received: March 4, 2008; In Final Form: April 4, 2008

G-quadruplexes are believed to be potential targets for therapeutic intervention and this has resulted in designing of various quadruplex interacting ligands. Moreover, reports about existence of quadruplex forming sequences across the genome have propelled greater interest in understanding their interaction with small molecules. An intramolecular quadruplex sequence can adopt different conformations, owing to different orientation of loops in the structure. The differences in the loop orientation can affect their molecular recognition. Herein, we have studied the interaction of 5,10,15,20-tetrakis(1-methyl-4-pyridyl)-21H, 23H-porphine (TMPyP4), a well-known G quadruplex binding ligand with three DNA quadruplexes differing in loop orientations. Results obtained from UV, ITC, and SPR studies have coherently revealed that the TMPyP4 molecule shows preferential binding to parallel G-quadruplex (*c-myc* and *c-kit*) over its antiparallel counterpart (human telomeric). The binding affinity for parallel quadruplex was (10^7) 1 order of magnitude higher than that for antiparallel DNA quadruplex (10^6). The study shows two binding modes, stronger binding (10^7) of TMPyP4 involving end stacking and a weaker external binding (10^6), while TMPyP4 shows only one binding mode with duplex with a binding affinity of the order of 10^6. Overall, the study emphasizes that differences in the loop orientation give rise to different conformations of quadruplex, which in turn govern its binding to small molecules, and thereby play a pivotal role in molecular recognition.

Introduction

G-quadruplexes are made up of stacked G-quartet subunits, wherein four coplanar guanines (G) are linked together by Hoogsteen hydrogen bonds.[1] In the past decade, there has been growing interest in the structure, molecular recognition, and function of these four-stranded DNA G-quadruplexes. The potential role of G-quadruplexes in vivo has been highlighted in the recent development of chemotherapeutic strategies designed to stabilize telomeric ends in G-quadruplex form using specific molecules, which in turn disables telomere maintenance in tumor cells.[2,3] The findings that quadruplex forming sequences occur in the promoter regions of several oncogenes such as *c-kit*,[4] *bcl-2*,[5] and *k-ras* [6]can lead us to identify the possible role of quadruplex structures in the manipulation of gene regulation. The discovery of proteins such as transcription factors, nucleases, and helicases that can bind to and even promote the formation of quadruplexes reinforce the speculated in vivo existence of quadruplexes.[7–9] As G-quadruplexes are present in the regulatory regions of several important genes that are involved in various cancers, they can act as attractive therapeutic targets. Several ligands including derivatives of acridines,[10–12] cationic TMPyP4,[13–19] ethidium,[20,21] anthraquinone,[22] perylene,[23] and telomestatin [24–29] have been investigated for their ability to bind to quadruplex thus interfering with its corresponding biological functions. Cationic TMPyP4 has been of particular interest in photodynamic cancer therapy,[30,31] largely because of its ability to accumulate to greater extent in tumor tissues more than in normal tissues. The planar arrangement of the aromatic rings in TMPyP4 analogs has led researchers to propose that such compounds might be able to bind to G-quadruplexes through interactive stacking with the G-tetrads. Two different G-quadruplex-binding models have been proposed for TMPyP4s. One model, based upon photocleavage data, predicts that TMPyP4 molecules stack externally with G-tetrads located at the ends of G-quadruplex,[32] while the other model based on molecular modeling and stoichiometry measurements suggests that TMPyP4 molecules intercalate between two G-tetrads.[33] Most recent report from crystallographic studies refute the intercalative mode.[34] Studies using tumor cell lines demonstrated that TMPyP4 has a retarding effect on cell growth, which is in accord with the telomerase inhibition data.[35] TMPyP4 also induces anaphase chromosomal bridges in sea urchins.[36] This result indicated that G-quadruplex-interactive compounds might target the telomeres directly inside cells. More than 150 TMPyP4 analogs have been screened using a cell-free telomerase assay and a DNA synthesis arrest assay.[37,38] Some of these compounds exhibited G-quadruplex interaction, while some others were completely devoid of such activity. Structure−activity relationship studies showed that the total charge, the side-chain length, and the hydrogen-bonds in the compounds are among the most important factors determining the interaction of these compounds with G-quadruplexes. Arthanari and co-workers reported increase in fluorescence intensity of porphyrins upon binding to G-quadruplexes.[39] They proposed that porphyrins could be used to screen other G-quadruplex-interactive agents by monitoring the replacement of TMPyP4 molecules from G-quadruplex DNA. Finally, Li and co-workers have shown that DNA aptamers that selectively bind to TMPyP4s fold to form a G-quadruplex structure.[40] TMPyP4 also down regulates the expression of the *c-myc* [41]and *k-ras*[6] proto-oncogenes by binding to the quadruplexes formed in their promoter sequences. Computational studies show that there are several thousands of putative quadruplex forming sites existing in the human genome. When every possible combination is considered, a survey of the ensemble database (V20 NCBI

* To whom correspondence should be addressed. Email: souvik@igib.res.in. Phone: +91-11-2766-6156. Fax: +91-11-2766-7471.

10.1021/jp711608y CCC: $40.75
Published on Web 06/14/2008

TABLE 1: Oligonucleotides Used in the Study

DNA sequence name	oligonucleotide sequence (5′−3′)	length
c-myc	GGGGAGGGTGGGGAGGGTGGGG	22
c-kit	GGGAGGGCGCTGGGAGGAGGG	21
telomeric	GGGTTAGGGTTAGGGTTAGGG	21
duplex	GCGCGAGAAGAAAAGAAAGCCGG CCGGCTTTCTTTTCTTCTCGCGC	23
hairpin duplex(For SPR)	Bio-TTTTTTTTTCGAATTCGTTTTTC GAATTCG	30
c-myc	Bio-TTTTTTTTTGGGGAGGGTGGGGA GGGTGGGG	31
c-kit	Bio-TTTTTTTTTGGGAGGGCGCTGGG AGGAGGG	30
telomeric	Bio-TTTTTTTTTGGGTTAGGGTTAGGG TTAGGG	30

assembly 34c) yields 5 713 900 possible potential quadruplex sequences in the human genome. However, this corresponds to a maximum of 375 157 distinct nonoverlapping potential quadruplex sequences.[42] In this context, the natural question is that whether the recognition capabilities of all the different quadruplexes will be identical or significantly variable. An intramolecular quadruplex sequence may be broken down to yield four equal sized G-tracts and distinct loop regions of varying length and base composition. The differences in the loop regions in terms of their length, base composition, and orientation in the quadruplex can affect its molecular recognition by targeted molecules. So, in this study, we have attempted to understand whether TMPyP4 can selectively distinguish between different putative quadruplexes with varying loop regions in the genomic system and its selectivity for quadruplex over duplex DNA. We have characterized the binding capabilities of TMPyP4 to quadruplex structures present in the promoter region of *c-myc* and *c-kit* and in the human telomeric region which display different loop orientation using spectroscopic and calorimetric techniques.

Materials and Methods

Materials. 5,10,15,20-Tetrakis(1-methyl-4-pyridyl)-21H, 23H-porphine (TMPyP4), was purchased in the form of tetra-p-tosylate salt from Sigma (USA). Concentrated TMPyP4 solution in distilled deionized water was stored in the dark at −20 °C to prevent photodegradation. Before experiments, the concentrated TMPyP4 was diluted to a buffer solution composed of 10 mM sodium cacodylate buffer and 100 mM KCl at pH 7.0. The concentration of TMPyP4 was determined by measuring the absorbance at 422 nm with an extinction coefficient of 2.26×10^5 M^{-1} cm^{-1}.[43] All the nucleotides were purchased from Microsynth of HPLC-purified grade. The sequences of the oligonucleotides used in these studies are presented in Table 1. Concentrations of oligonucleotide solutions were determined from absorbance at 260 nm using molar extinction coefficient at 260 nm of 22.70×10^4 M^{-1} cm^{-1}, 21.32×10^4 M^{-1} cm^{-1}, and 22.85×10^4 M^{-1} cm^{-1} for *c-myc*, *c-kit*, and telomeric sequences, respectively. These values were calculated by extrapolation of tabulated values of the dimers and monomer bases[44] at 25 °C, using procedures reported earlier.[45] All other reagents were analytical grade. Milli Q water was used through out all the experiments. All experiments were done in 10 mM sodium cacodylate buffer, pH 7.0, containing 100 mM KCl at 25 °C unless mentioned otherwise. For all the studies, we used preformed quadruplex obtained by heating the solutions containing the G-rich sequences in 100 mM KCl to 100 °C for 5 min and gradually cooling down to 10 °C at the rate of 0.2 °C min^{-1} followed by overnight incubation.

UV−Vis Absorption Titration Experiments. Absorption spectra were measured on a Cary100 UV−vis double-beam spectrophotometer with a 1 cm path-length quartz cell. UV−vis absorption titrations were carried out by the stepwise addition of G-quadruplex solutions to a cell containing 1.33 μM TMPyP4, and absorption spectra were recorded in the 350−500 nm range at 25 °C. The titration was terminated when the wavelength and intensity of the absorption band for TMPyP4 did not change any more upon three successive additions of G-quadruplexes. Titration data was used to construct Scatchard plots by plotting r/C_f versus r for analysis, where r is the number of ligand molecules bound per mole of quadruplex and C_f is the free TMPyP4 concentration. Reverse titrations were also carried out by the stepwise addition of TMPyP4 solution to a cell containing 3 μM of each G-quadruplex solution. All the experiments were carried out in triplicates and the standard error was calculated.

In case of normal titrations, the concentrations of free TMPyP4 (C_f) and bound TMPyP4 (C_b) are calculated using $C_f = C(1 - \propto)$ and $C_b = C_T - C_f$, respectively, where C_T is the total TMPyP4 concentration (1.33 μM). The fraction of bound TMPyP4 ($\propto$) was calculated using the equation, $\propto = (A_f - A)/(A_f - A_b)$, where A_f and A_b are the absorbance of the free and fully bound TMPyP4 at the Soret maximum (422 nm) of TMPyP4, respectively, and A is the absorbance (422 nm) at any given point during the titration. The percent hypochromicity of the Soret band of TMPyP4 can be calculated using the percent hypochormicity $= [(\epsilon_f - \epsilon_b)/\epsilon_f] \times 100$, where $\epsilon_b = A_b/C_b$ and $\epsilon_f = A_f/C_f$.

In case of reverse titrations, a constant concentration of the quadruplex DNA was treated with increasing concentration of the TMPyP4. The amount of free and bound TMPyP4 was determined. Following each addition of drug to the quadruplex solution (3 μM), from the absorbance at the isosbestic point at 434 nm, the total drug concentration present was calculated as $C_T = A_{434}/\epsilon_{434}$. This quantity was used to calculate the expected absorbance at 422 nm, $A_{exp} = C_T\epsilon_{422}$. The difference in A_{exp} and the observed absorbance (A_{obs}) was then used to calculate the amount of bound TMPyP4 as $C_b = A/\Delta\epsilon = (A_{exp} - A_{obs})/(\epsilon_f - \epsilon_b)$.The amount of free drug was determined by difference, $C_f = C_T - C_b$. The extinction coefficient of the completely bound TMPyP4 was determined by adding a known quantity of TMPyP4 to a large excess of quadruplex DNA and on the assumption of total binding, $\epsilon_b = A_{422}/C_T$. Alternatively, the absorbance of a known quantity of TMPyP4 was monitored at 422 nm while adding known amounts of quadruplex until no further change in absorbance was observed. Both these protocols gave identical values within experimental errors. Binding data obtained from spectrophotometric titration of increasing concentrations of TMPyP4 to a fixed concentration of quadruplex DNA were used to construct Scatchard plot of r/C_f versus r, where r is the number of ligand molecules bound per mole of quadruplex and C_f is the free TMPyP4 concentration.

As the binding isotherm for the interaction of TMPyP4 with different quadruplexes obtained here were nonlinear, so to evaluate the binding parameters with higher accuracy, several fitting models were used as described below. Data were initially fitted using the simpler, linear Scatchard equation:

$$r/C_f = K(n - r) \quad (1)$$

where r is the number of moles of TMPyP4 bound to 1 mol of G-quadruplex (C_b/C_{quad}), n is the stoichiometry of TMPyP4-quadruplex interaction, C_f is the free ligand concentration, and K is the affinity of ligand for the binding site. Binding data

were also fitted by nonlinear least-squares analysis to a neighbor exclusion model,[46] which considers occupancy of multiple binding sites:

$$r/C_f = K(1 - pr)[(1 - pr)/(1 - (p - 1)r)] \quad (2)$$

where K is the intrinsic equilibrium binding constant and p is an exclusion parameter that defines the number of ligand molecules bound per DNA quadruplex. Then data were fitted using the two binding-site Scatchard equation as follows:

$$r/C_f = n_1K_{d1}/(1 - K_{d1})C_f + n_2K_{d2}/(1 + K_{d2})C_f \quad (3)$$

K_{d1} and K_{d2} are the quadruplex-TMPyP4 binding site dissociation constant for the sites and n_1 and n_2 are the stoichiometries of TMPyP4−quadruplex interaction.

Binding data was further plotted as r vs C_f and analyzed by nonlinear regression using the one-site rectangular hyperbolic binding isotherm according to

$$r = (n_1 \times C_f)/(K_d + C_f) \quad (4)$$

where r the number of moles of TMPyP4 bound to 1 mol of G-quadruplex (C_b/C_{quad}), n_1 is the stoichiometry of TMPyP4-quadruplex interaction, C_f is the free TMPyP4 concentration, and K_d is the quadruplex-TMPyP4 dissociation constant and $K_d = 1/K_a$.

The final method utilized to analyze binding data was a two-site nonlinear regression method using the two-site rectangular hyperbolic binding isotherm according to

$$r = (n_1 \times C_f)/(K_{d1} + C_f) + (n_2 \times C_f)/(K_{d2} + C_f) \quad (5)$$

where r the number of moles of TMPyP4 bound to 1 mol of G-quadruplex (C_b/C_{quad}), n_1 and n_2 are the stoichiometries of TMPyP4-quadruplex interaction, C_f is the free TMPyP4 concentrations, and K_{d1} and K_{d2} are the quadruplex-TMPyP4 equilibrium dissociation constants. Origin 7.0 was used for all the fitting analysis.

Isothermal Titration Calorimetry (ITC). ITC measurements were carried out in a VP- ITC titration calorimeter (MicroCal, Northampton, MA). Before loading, the solutions were thoroughly degassed. The reference cell was filled with the degassed buffer. The preformed quadruplex (10 μM) was kept in the sample cell, and TMPyP4 (146−500 μM) in the same buffer was filled in the syringe of volume 300 μl. TMPyP4 solution was added sequentially in 6−10 μl aliquots (for a total of 25−40 injections, 20 s duration each) at 4 min intervals at 25 °C. Sequential titrations were performed to ensure full occupancy of the binding sites by loading and titrating with the same ligand without removing the samples from the cell until the titration signal was essentially constant. The heats of dilution were determined in parallel experiments by injecting TMPyP4 solution of same concentration in the same buffer. The respective heats of dilution were subtracted from the corresponding binding experiments prior to curve fitting. Typically, three replicate titration experiments were performed. Due to the non-sigmoidal shape of the thermograms and the obvious presence of at least two independent binding processes, the thermograms (integrated heat/injection data) obtained in ITC experiments were fit with two independent sites model in Origin7.0. The experiments were carried out in triplicates and the standard error was calculated.

Surface Plasmon Resonance Study (SPR). SPR measurements were performed with BIAcore 2000 (BIAcore Inc.) system using streptavidin-coated sensor chips (Sensor chip SA, BIAcore Inc.). All the 5′- biotinylated sequences have T9 linker, as tabulated in Table 1, and were heated to 95 °C and annealed by slow cooling to form quadruplex in filtered and degassed 10 mM HEPES buffer with 100 mM KCl with 0.005% surfactant IGEPAL, pH 7.4. Flow cells 2 and 4 were used as sample flow cells for the immobilization of the biotinylated oligos. Flow cells 1 and 3 were left blank as controls to account for any signal generated owing to bulk solvent effect or any other effect not specific to the DNA interaction, which was subtracted from the signal obtained in flow cells 2 and 4, respectively. All experiments were performed at 25 °C using running buffer (filtered and degassed 10 mM HEPES with 100 mM KCl and 0.005% surfactant IGEPAL) at pH 7.4. Oligonucleotide immobilized surface was exposed to the running buffer for at least 2 h at a flow rate of 20 μl min^{-1} for attaining baseline stability. Analyte solutions at different concentrations (2.5×10^{-8} M to 3.2×10^{-6} M) were prepared in the running buffer and were injected (at 20 μl min^{-1} for 300 s) in random series to avoid any systematic error. Following this, dissociation from the surface was monitored for 300 s in running buffer. Regeneration was done using 1 M NaCl in 50 mM NaOH. Analysis of the binding sensorgrams were carried out using two independent binding sites model using BIA evaluation software 3.1. The experiments were carried out in triplicates and the standard error was calculated.

Results

Equilibrium Binding Studies by UV−Vis Method. UV−vis absorption spectroscopy is routinely used to understand the DNA binding behavior of a ligand. In the present study, we have focused on the binding of TMPyP4 to three different quadruplex forming sequences derived from the promoter regions of *c-myc* and *c-kit* proto-oncogenes and from human telomeric repeat as well as to duplex DNA. Figure 1 shows the changes in the absorption spectra of TMPyP4 when titrated against increasing amounts of DNA (G-quadruplex and duplex individually). The UV absorption profile of TMPyP4 saturated with the different DNA sequences has been summarized in the Table 2. In case of quadruplexes, interaction of TMPyP4 with *c-myc* and *c-kit* produced up to 56% hypochromicities along with a red shift of up to 17 nm, whereas with telomeric quadruplex, there was only 43% hypochromicity along with 14 nm shift in the Soret band of TMPyP4. A sharp isosbestic point at 434 nm was seen in all the cases (Figure 1). The change in the absorption at 422 nm in the absorption spectra of TMPyP4 was used to construct the Scatchard plots (r/C_f *vs* r). The Scatchard plots so obtained were all nonlinear and upwardly concave, which clearly indicate more than one binding site for TMPyP4 in all the quadruplexes (Supporting Information Figure 1). Scatchard plots are linear only for binding to independent and equivalent sites; any curvature in the plots indicates the existence of more than one type of binding site, ligand-ligand interactions, or neighbor exclusion effects.[46]

To decipher whether curvature in Scatchard plot was due to two binding sites or due to neighbor exclusion effects, data was analyzed using different fitting models. Data was initially analyzed using the simpler, linear Scatchard equation (eq 1 in Material and Methods), which did not give good fitting results. This was followed by nonlinear least-squares analysis that considers occupancy of multiple binding sites with cooperative behavior using eq 2 in Material and Methods, which also did not fit well. Reverse titrations, whereby the quadruplex sequence was titrated against increasing amounts of TMPyP4, were conducted to obtain the r/C_f values for the lower values of r, which were not achievable with direct titrations. Upon analysis, the data points again showed a nonlinear and concave curve and could not be fitted with eq 2, justifying more than one

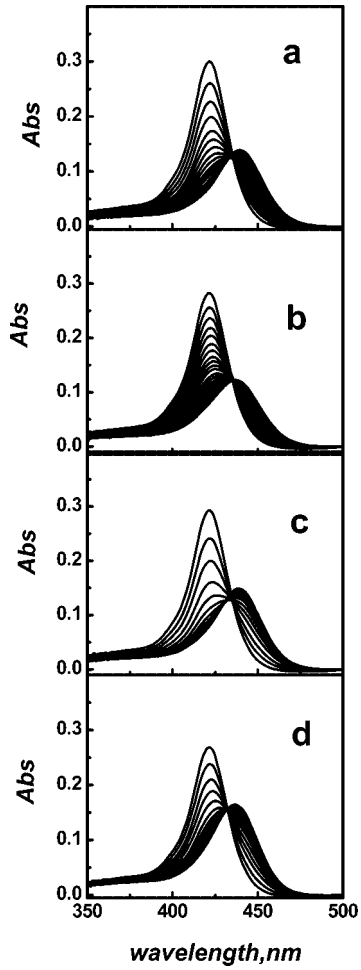

Figure 1. UV−vis absorption titration spectra of 1.33μM TMPyP4 with (a) *c-myc*, (b) *c-kit*, (c) telomeric G-quadruplexes, and (d) 23-mer duplex DNA in 10 mM sodium cacodylate buffer, pH 7.0, containing 100 mM KCl at 25 °C.

binding sites in case of quadruplexes (Supporting Information Figure 2). In case of hyperbolic upward-curved Scatchard plots, it is possible to dissect the plots into two components and can be analyzed using eq 3. No advantage was also observed in terms of better fitting of the data using two component model (eq 3 in Material and Methods). Binding data was then plotted as r vs C_f and analyzed by nonlinear regression. We fitted the data to both single site rectangular hyperbola model (eq 4 in Material and Methods) as well as the dual site rectangular hyperbola model (eq 5 in Material and Methods). Finally, better residuals and the comparatively better χ^2 values with the dual hyperbola model lead us to conclude that this was the more suitable model for data fitting to obtain the binding parameters (panels a−c in Figure 2). The binding parameters have been summarized in the Table 2. The binding affinity for first (K_{a1}) and second site (K_{a2}) were 9.4(±0.5) × 10^7 M^{-1} and 1.1(±0.05) × 10^6 M^{-1} for *c-myc*, 1.4(±0.07) × 10^7 M^{-1} and 0.5(±0.02) × 10^6 M^{-1} for *c-kit*, and 5.0(±0.25) × 10^6 M^{-1} and 1.1(±0.05) × 10^6 M^{-1} for telomeric quadruplex. The stoichiometries of interaction were 1.0, 0.9, and 1.1 for the first interaction, while they were 1.9, 1.8, and 1.7 for the second binding to *c-myc*, *c-kit*, and telomeric quadruplex, respectively. Successive addition of duplex DNA until saturation of TMPyP4 brings about a red shift of 14 nm in the Soret band from 422 nm 436 nm, simultaneous with a 35% hypochromicity, which suggests an interaction of TMPyP4 with DNA.The distinct isosbestic point at 434 nm is suggestive of equilibrium in the binding process. The duplex data showed good linear fitting in Scatchard plot (r/C_f *vs* r) and suggested a single binding site (monoexponential) for TMPyP4 (panel d in Figure 2), with a binding affinity (K_a) of 5.0(±0.25) × 10^6 M^{-1} and stoichiometry (n) value of 7 (Table 2).

ITC Based Thermodynamic Studies. With recent advancement in the sensitivity and reliability of the calorimeter, ITC has become an important tool for the direct measurement of thermodynamic parameters in various biological interactions. ITC yields thermodynamic parameters such as Gibbs free energy change (ΔG), enthalpy change (ΔH), and entropy change (ΔS) along with the number of binding sites (n) in a single experiment. Figure 3 shows typical integrated heat data for the titration of all the quadruplexes and duplex DNA with TMPyP4. The ITC data for the TMPyP4-quadruplex and TMPyP4-duplex complexes are presented in Table 3. The microcalorimetric signal and integrated heat data were biphasic and were consistent with at least two independent binding processes occurring during complex formation for all the quadruplexes (panels a−c in Figure 3). Out of all the different binding models, the model with two binding modes involving "two independent sites" is the simplest model that can fit the titration data for TMPyP4−quadruplex interaction with best fitting and relatively good χ^2 values. Data obtained shows that two binding modes for the TMPyP4−quadruplex interaction were significantly different. TMPyP4 binding to the higher affinity quadruplex site, K_{a1} of 7.0(±0.7) × 10^7 M^{-1}, was approximately 70 times stronger than binding to the lower affinity site, K_{a2} of 1(±0.1) × 10^6 M^{-1}, for the *c-myc* quadruplex. Similarly, K_{a1} value of 1.5(±0.15) × 10^7 M^{-1} for *c-kit* and 4.0(±0.4) × 10^6 M^{-1} for telomeric were found to be 15 and 8 times higher than K_{a2} values of 1(±0.1) × 10^6 M^{-1} and 0.5(±0.5) × 10^6 M^{-1} for lower affinity site, respectively (Table 3). The higher binding affinity values for the stronger binding site for the *c-myc* and *c-kit* quadruplexes as compared to the telomeric quadruplex is in concordance with the UV binding data (Table 2). The stoichiometries of interaction for the first and second binding were found to be 1 and 2, respectively, for all the quadruplexes Moreover, the duplex form of DNA showed a monophasic and single site binding only (panel d in Figure 3). The ITC thermograms exhibited a single binding site of TMPyP4 for the duplex form of DNA with K_a value of 1.0(±0.1) × 10^6 M^{-1} and n value of 5 (Table 3). The two binding modes have markedly different energetic profiles. The binding enthalpy change was negative in all the cases suggesting that the binding process is essentially exothermic. In case of quadruplexes the binding enthalpy (ΔH) for the stronger binding was −7.5(±0.7) kcal mol^{-1} for *c-myc*, −3.0(±0.3) kcal mol^{-1} for *c-kit*, and −1.9(±0.2) kcal mol^{-1} for telomeric quadruplex. For the weaker binding mode, the ΔH values were also exothermic, viz., −10.2(±1.0) kcal mol^{-1} for *c-myc*, −7.9(±0.8) kcal mol^{-1} for *c-kit*, and − 4.2(±0.4) kcal mol^{-1} for telomeric quadruplex. The entropy (ΔS) values for the stronger binding were found to be 10.4(±1.0), 22.8(±2.3), and 23.8(±2.4) cal mol^{-1} K^{-1} for *c-myc*, *c-kit*, and telomeric quadruplex, respectively, while for the weaker binding, the entropy (ΔS) value was −6.7(±0.7) cal mol^{-1} K^{-1} for *c-myc*, 1.0(±0.1) cal mol^{-1} K^{-1} for *c-kit*, and 23.0(±2.3) cal mol^{-1} K^{-1} for telomeric quadruplex. The overall ΔG_1 of TMPyP4 binding for all the quadruplexes ranges from −9.0(±0.9) to −10.6(±1.1) kcal mol^{-1}, while ΔG_2 values ranges from −7.8(±0.8) to −8.2(±0.8) kcal mol^{-1}. As shown in Figure 3 (panel d) and represented in Table 3, the data for the TMPyP4−duplex interaction showed only single binding mode with ΔH value of

TABLE 2: Binding Parameters Obtained From UV−Vis Titration Experiments in 10 mM Sodium Cacodylate Buffer, pH 7, 100 mM KCl at 25 °C[a]

DNA	K_{a1} (M^{-1})	n_1	K_{a2} (M^{-1})	n_2	% hypochromicity
c-myc Q	9.4 (±0.5) × 10^7	1.0	1.1 (±0.05) × 10^6	1.9	56
c-kit Q	1.4 (±0.07) × 10^7	0.9	0.5 (±0.02) × 10^6	1.8	49
telomeric Q	5.0 (±0.25) × 10^6	1.1	1.1 (±0.05) × 10^6	1.7	43
duplex	5.0 (±0.25) × 10^6	7.0			35

[a] K_{a1} is the binding affinity of TMPyP4 for the stronger binding site in quadruplex, K_{a2} is the binding affinity of TMPyP4 for the weak binding site in quadruplex, and n_1 and n_2 are the stoichiometries of strong and weak binding respectively. Hypochromicity (%) is calculated as described in Materials and Methods. The binding parameters obtained were ±5% error.

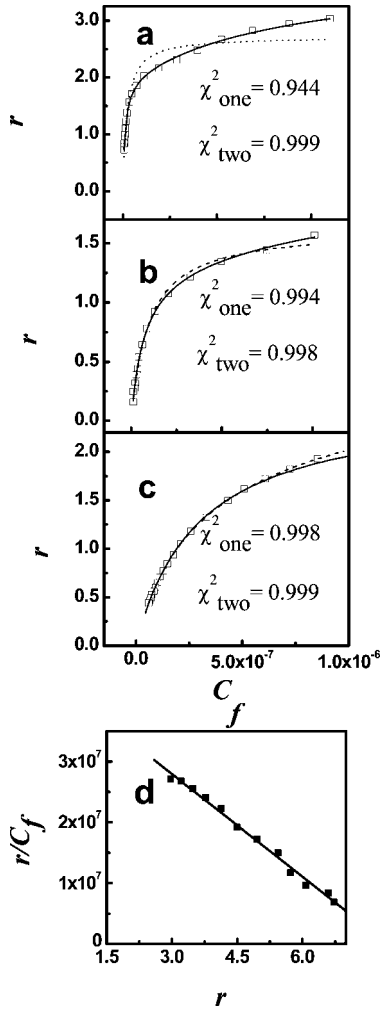

Figure 2. Plots of *r* (moles of bound TMPyP4/1 mol of G-quadruplexes or duplex) versus C_f (concentration of free TmPyP4) for the absorption titrations of TMPyP4 with different G-quadruplexes (a) *c-myc*, (b) *c-kit*, and (c) telomeric, and (d) r/C_f vs *r* plot for duplex. The resulting data were analyzed by either one-site nonlinear regression method or two-site nonlinear regression method (eq 4 and eq 5, respectively, as described in Material and Methods) and corresponding $\chi 2$ values are shown in the plot.

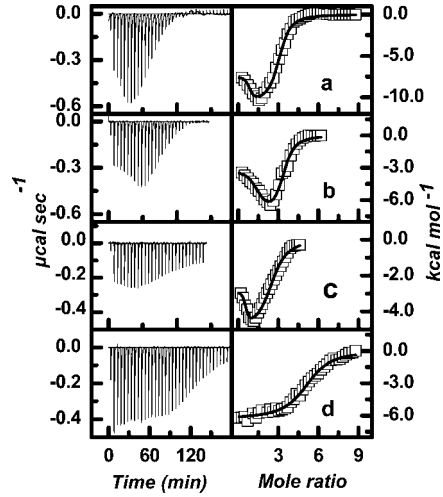

Figure 3. ITC profile for the TMPyP4 binding to (a) *c-myc*, (b) *c-kit*, (c) telomeric quadruplexes, and (d) duplex DNA in 10 mM sodium cacodylate buffer, pH 7.0, containing 100 mM KCl at 25 °C. Data were fitted to " two independent sites" binding model using Origin 7.0 software.

−6.3(±0.6) kcal mol^{-1} and ΔS value of 6.0(±0.6) cal mol^{-1} K^{-1} with the overall ΔG value of −8.1(±0.8) kcal mol^{-1} (Table 3).

Surface Plasmon Resonance Based Kinetic studies. SPR yields direct information on the binding of the ligands to both the quadruplexes and duplex DNA and thus enables the determination of the ratio of the two equilibrium-binding constants (K_{G4DNA}/K_{dsDNA}, Table 4), which is a measure of G-quadruplex binding selectivity. Fitting of binding curves (Figure 4) using the two binding site model suggested that TMPyP4 had a stronger binding site of the order of 10^7 on the quadruplex along with a weaker secondary binding interaction of the order of 10^6 (Table 4). The observed association rate constants were concentration-dependent, but the dissociation rate constants were independent of ligand concentration. The k_{a1}, k_{d1} and k_{a2}, k_{d2} values contribute toward the respective association constants K_{a1} and K_{a2} for the two binding modes obtained in the TMPyP4−quadruplex interaction. We observed that for all the quadruplexes the k_{d1} and k_{d2} followed the same order (10^{-3}) while the k_{a1} values were one order higher than k_{a2} (Table 4). The binding affinity (K_{a1}) obtained for the stronger binding was 3.0(±0.4) × 10^7 M^{-1} for *c-myc* quadruplex, 1.5(±0.2) × 10^7 M^{-1} for *c-kit* quadruplex, and 5.0(±0.7) × 10^6 M^{-1} for telomeric quadruplex. However, the binding affinity (K_{a2}) for the second binding mode was 4.0(±0.6) × 10^6 M^{-1} for *c-myc* quadruplex, 3.7(±0.6) × 10^6 M^{-1} for *c-kit* quadruplex, and 2.0(±0.3) × 10^6 M^{-1} for telomeric quadruplex. Moreover, in case of parallel *c-myc* and *c-kit* quadruplex, the association rate constant k_{a1} value for the stronger binding of TMPyP4 was one order higher than k_{a1} value for the TMPyP4−telomeric quadruplex interaction (Table 4). In the concentration range examined, TMPyP4 bound more tightly to quadruplex DNA in comparison to hairpin duplex DNA. Binding affinity value, K_a determined from the steady state region of sensorgram for duplex was 5(±0.7) × 10^6 M^{-1} with k_{a1} and k_{d1} values of 5(±0.7) × 10^5 M^{-1} sec^{-1} and 1(±0.2) × 10^{-1} sec^{-1}, respectively (Table 4).

Discussion

High red shifts (14−17 nm) and substantial hypochromicities (43−56%, though only 35% for duplex) in the Soret band of

TABLE 3: Thermodynamic Parameters Obtained from ITC Experiments Conducted in 10 mM Sodium Cacodylate Buffer, pH 7, 100 mM KCl at 25 °C[a]

DNA	ΔH_1 (kcal mol^{-1})	K_{a1} (M^{-1})	ΔS_1 (cal mol^{-1} K^{-1})	ΔG_1 (kcal mol^{-1})	n_1	ΔH_2 (kcal mol^{-1})	K_{a2} (M^{-1})	ΔS_2 (cal mol^{-1} K^{-1})	ΔG_2 (kcal mol^{-1})	n_2
c-myc Q	−7.5 (±0.7)	7.0 (±0.7) × 10^7	10.4 (±1.0)	−10.6 (±1.1)	1	−10.2 (±1.0)	1.0 (±0.1) × 10^6	−6.7 (±0.7)	−8.2 (±0.8)	2
c-kit Q	−3.0 (±0.3)	1.5 (±0.15) × 10^7	22.8 (±2.3)	−9.8 (±1.0)	1	−7.9 (±0.8)	1.0 (±0.1) × 10^6	1.0 (±0.1)	−8.2 (±0.8)	2
telomeric Q	−1.9 (±0.2)	4.0 (±0.4) × 10^6	23.8 (±2.4)	−9.0 (±0.9)	1	−4.2 (±0.4)	0.5 (±0.05) × 10^6	23.0 (±2.3)	−7.8 (±0.8)	2
duplex	−6.3 (±0.6)	1.0 (±0.1) × 10^6	6.0 (±0.6)	−8.1 (±0.8)	5					

[a] Thermodynamic parameters were obtained for TMPyP4 binding to the preformed quadruplexes and duplex DNA at 25 °C. Quadruplex concentration in the cell was 10 μM and the TMPyP4 concentration in the syringe was (146−500) μM. ΔG was determined using the relation $\Delta G = -RT\ln K$, where R is universal gas constant, T is temperature, and K is the binding affinity for TMPyP4−quadruplex interaction. ΔH_1 and ΔH_2 correspond to the binding enthalpy change for the strong and weak binding, respectively, ΔS_1 and ΔS_2 correspond to the binding entropy change for the strong and weak binding, respectively, ΔG_1 and ΔG_2 correspond to the free energy change for the strong and weak binding, respectively, K_{a1} and K_{a2} correspond to the binding affinity of TMPyP4 for the strong and weak binding sites on DNA, respectively, and n_1 and n_2 are the respective stoichiometries for strong and weak binding. The parameters obtained were ±10% error.

TABLE 4: Kinetic Parameters Obtained from SPR in 10 mM HEPES Buffer, pH 7.4, 100 mM KCl at 25 °C[a]

DNA	k_{a1} (M^{-1}sec^{-1})	k_{d1} (sec^{-1})	K_{a1} (M^{-1})	k_{a2} (M^{-1} sec^{-1})	k_{d2} (sec^{-1})	K_{a2} (M^{-1}sec^{-1})	K_{G4a1}DNA/K_{ds}DNA
c-myc Q	1.5 (±0.2) × 10^5	5.0 (±0.7) × 10^{-3}	3.0 (±0.4) × 10^7	8.0 (±1.0) × 10^3	2.0 (±0.3) × 10^{-3}	4.0 (±0.6) × 10^6	1−6
c-kit Q	6.0 (±0.9) × 10^4	4.0 (±0.6) × 10^{-3}	1.5 (±0.2) × 10^7	1.5 (±0.2) × 10^4	4.0 (±0.6) × 10^{-3}	3.7 (±0.6) × 10^6	
telomeric Q	1.5 (±0.2) × 10^4	3.0 (±0.4) × 10^{-3}	5.0 (±0.7) × 10^6	4.0 (±0.6) × 10^3	2.0 (±0.3) × 10^{-3}	2.0 (±0.3) × 10^6	
duplex	5.0 (±0.7) × 10^5	1.0 (±0.2) × 10^{-1}	5.0 (±0.7) × 10^6				

[a] k_{a1} and k_{d1} corresponds for the association and dissociation rate constants for strong binding respectively, while k_{a2} and k_{d2} corresponds for the association and dissociation rate constants for weak binding, respectively. K_a is equilibrium association constant for TMPyP4−DNA interaction obtained by k_a/k_d. K_{a1} and K_{a2} correspond for equilibrium binding constant for strong and weak binding site, obtained by k_{a1}/k_{d1} and$k_{a2}/k_{d2,}$ respectively. K_{G4a1}DNA is the stronger binding affinity for TMPyP4−quadruplex interaction. K_{ds}DNA is the binding affinity for TMPyP4−duplex interaction. Error levels for k_a, k_d, and K_a values were ±15% error.

TMPyP4 obtained in UV titration experiments clearly indicate that TMPyP4 binds to G-quadruplexes as well as Duplex DNA. Similar observations were reported for TMPyP4 interactions with quadruplex,[14,15,18] duplex DNA,[18] and RNA duplexes.[47] The Scatchard plots as obtained were nonlinear and upwardly concave suggesting more than one binding sites in the interaction of TMPyP4 with quadruplexes. Scatchard plots are linear only for binding to independent and equivalent sites, and any curvature in the plots indicates the existence of more than one type of binding site, ligand−ligand interactions, or neighbor exclusion effects.[46] The two binding modes involving independent binding sites for TMPyP4-quadruplex interaction in our study can be discussed in the light of available literature. Phan et al.[48] showed through NMR study that TMPyP4 binds to quadruplex at one site by stacking on the top of G-tetrad at [TMPyP4]/[quadruplex] ratio of 0.5−1.0. Recently, the crystal structure of TMPyP4-quadruplex complex as documented by Neidle and co-workers[34] demonstrated two binding modes involving two different sites at higher [TMPyP4]/[quadruplex] ratio ranging from 1:1 to 5:1. Our studies also indicate that TMPyP4 binding involves two binding modes and, moreover, the binding sites are independent of each other. Among these two modes, we suggest that one is the end stacking mode, wherein the aromatic planar rings of TMPyP4 stack over the end quartet, while the second one is of external binding, whereby the TMPyP4 molecule interacts with the quadruplex from outside the tetrads stacked externally onto bases at the edges of the loops, as observed in the crystal structure of TMPyP4−quadruplex complex reported by Neidle and co-workers.[34] It has been a raging debate for years that intercalation of TMPyP4 between the tetrads is one of the TMPyP4 binding mode, which is characterized by high hypochromicities and large bathochromic shifts.[18] Our results which do show hypochromicities and bathochromic shifts may impulsively resemble the intercalative mode because data are significantly different from groove binding and thus may falsely lead one to conclude intercalation. Chalikian et al. have also demonstrated using UV as well as CD studies that intercalation is accompanied by high hypochromicities and large bathochromic shifts along with a negative induced CD band in the Soret region of TMPyP4.[47] They have argued that modest shifts in the Soret band correspond to binding modes other than intercalation or groove binding. Moreover, crystallographic studies by Neidle and co-workers have also shown that intercalation is clearly not the mode of interaction of TMPyP4 with the quadruplex structures.[34]So, we concluded that intercalation is not the binding mode in this scenario. The two binding modes implicated are the end stacking shown by the high bathochromicity and the hypochromic shifts (which happens to be the stronger binding) and the one represented in the lower affinity, which is of external binding.

NMR studies, in potassium solution, conducted by Ambrus et al.[49] reports that the *c-myc* G-quadruplex structure adopts an intramolecular parallel-stranded quadruplex conformation with three guanine tetrads and three side loops, including two single-nucleotide side loops and one double-nucleotide side loop that connect the four guanine strands. The three side loops are very stable and well-defined. Another report by Phan et al.[50] showed that *c-myc* sequence containing sets of G-stretches form intramolecular propeller-type parallel-stranded G-quadruplexes in K^+ containing solution. The two structures, chair and basket form involve a core of three stacked G-tetrads formed by four parallel G-stretches with all antiguanines and three double-chain-reversal loops bridging three G-tetrad layers. The central loop contains two or six residues, while the two other loops contain only one residue. The *c-kit* NMR structure in the potassium solution represents a snapback parallel folded topology.[51] There are four loops: two single-residue double-chain-reversal loops, a two-residue loop, and a five-residue stem-loop, with base-pairing alignments. NMR based literature reveals that human telomeric quadruplex sequence forms a well defined basket type intramolecular G-quadruplex in the presence of Na^+ ion,[52] while the same sequence assumes multiple interconvertible conformations, comprising of the antiparallel and the hybrid-type G-quadruplexes, in the presence of K^+ ions.[53] The antiparallel quadruplex can further exist in two forms, namely, the basket-type and the chair-type. Since these two forms give spectrally

SCHEME 1: Scheme Showing Loop Orientation of Respective Quadruplex Structures along with the Probable TMPyP4 Binding Sites[a]

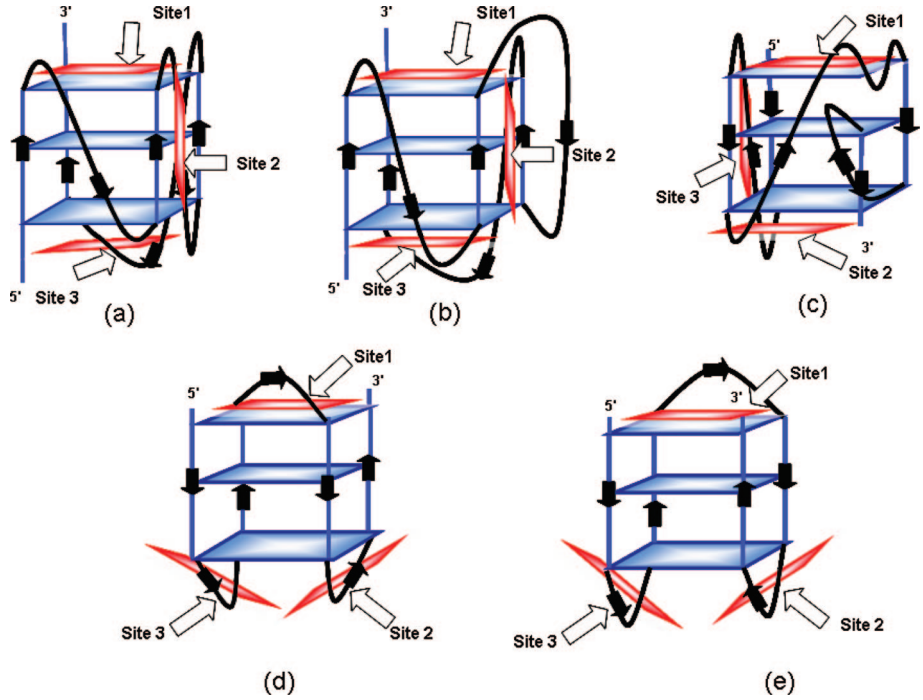

[a] (a) and (b) correspond to parallel *c-myc* quadruplex structure, (c) represents parallel *c-kit* quadruplex structure, and (d) and (e) represent the chair and basket form of antiparallel telomeric structure in the presence of K^+ ions. The arrows shows loop orientation. TMPyP4 is shown in red. Strong binding arises due to end stacking of TMPyP4 to site 1, while external binding of TMPyP4 to both sites 2 and 3 may contribute towards weaker binding mode.

indistinguishable signals in CD data, it becomes difficult to comment on actual conformation existing in the presence of K^+ ions.[54,55] Previous in vitro and simulation studies support the existence of chair-type conformation in presence of K^+ ion.[54–56] However, no solution structure is available for the 21 mer or 22 mer human telomeric quadruplex in the presence of K^+ ions. The CD analysis also shows predominant parallel conformation for *c-myc* and *c-kit* quadruplexes in the K^+ solution, while telomeric quadruplex in the presence of K^+ ions shows antiparallel conformation (Supporting Information Figure 3). Using available solution structure of *c-myc*, *c-kit* and proposed telomeric structure in literature, we have formulated an elemental scheme to demonstrate the quadruplex−TMPyP4 interaction. Our spectroscopic and calorimetric results show that all the three quadruplex have two different binding modes, involving strong binding with K_a of 10^7 and weak binding of the order 10^6 with binding stoichiometries 1 and 2, respectively. In our scheme 1, we have illustrated the binding mode of TMPyP4 to the different quadruplex structures. The stronger binding affinity of TMPyP4 obtained for both the *c-myc* and *c-kit* parallel quadruplexes was due to the end stacking at site 1 (Scheme 1a−c). However, in case of antiparallel telomeric quadruplex, the presence of diagonal and lateral loops (Scheme 1d,e) weakens the end stacking of TMPyP4 at site 1, thereby resulting in the lower K_a of 10^6 as compared to K_a of 10^7 in the cases of parallel *c-myc* and *c-kit* quadruplex structures, which do not have diagonal and lateral loops (Scheme 1a−c). The external binding at site 2 and 3 contributes to the second weaker binding mode in all the three quadruplexes.

Our results indicate that TMPyP4 binds with a higher affinity to parallel *c-myc* and *c-kit* quadruplexes when compared to a telomeric quadruplex adopting antiparallel and mixed hybrid conformation in the K^+ ion containing solution (Table 2). The binding affinities for the strong binding site in case of *c-myc* and *c-kit* quadruplexes with parallel conformation were also 1 order of magnitude more than the duplex DNA as compared to the antiparallel telomeric quadruplex (Table 2). This represents that TMPyP4 shows 1 order of magnitude higher binding toward parallel quadruplex over duplex DNA in comparison to antiparallel quadruplex. The stoichiometries indicate that each equivalent of duplex DNA can bind up to 7 equiv of TMPyP4. While in case of quadruplexes, the stoichiometry of the interaction was up to only 3 equiv of TMPyP4 for each equivalent of quadruplex showing the hindrance to interaction offered by the loops on the edges of the quartets in the secondary structure.

For a better understanding about the multiple binding sites and varied stoichiometries for TMPyP4 as well as to obtain the thermodynamic parameters involved in the interaction of TMPyP4 with different G4 quadruplexes as well as with the duplex DNA, the ITC studies were conducted. ITC experiments of quadruplexes and duplex DNA with TMPyP4 conducted at 25 °C exhibit monophasic binding for the duplex as against two independent binding processes for the quadruplexes. The thermodynamic profiles of TMPyP4 binding to quadruplexes for the two binding sites are very different. The association of TMPyP4 with all the DNA sequences exhibited negative changes in the binding enthalpies. The study shows that stronger binding of TMPyP4 by stacking at ends is enthalpically less favorable and entropically more favorable while the second weaker external binding is enthalpically more favorable and entropically less favorable for *c-myc* and *c-kit* quadruplex. Contrarily, in case of telomeric quadruplex, the end stacking as well as external binding TMPyP4 is both enthalpically and entropically favorable. This difference in the energetic profile for the TMPyP4 binding obtained for different quadruplexes can be attributed to the different conformations adopted by telomeric quadruplex (antiparallel) in comparison to *c-myc* and

c-kit quadruplex (parallel) as discussed above. We have also compared the binding of TMPyP4 to duplex. The TMPyP4-duplex interaction showed single binding favored by both enthalpy and entropy (Table 3).

The binding affinity obtained from SPR data analysis (Table 4) was in coherence with the UV and ITC data showing two binding modes for TMPyP4 interaction with all the three quadruplexes (Table 2 and 3). The data presented in Table 4 showed that there are two different binding sites, one showing stronger binding and the other weaker one with binding affinities of the order of 10^7 and 10^6, respectively. The kinetics of interaction can be interpreted in terms of association and dissociation rate constants, k_a and k_d, respectively. The k_{d1} and k_{d2} values among all the quadruplexes for both the binding sites are quite close and follow the same order of 10^{-3} (Table 4). There was an increase of 1 order of magnitude in the association rate constant, k_{a1}, for the stronger binding site over k_{a2} value, as illustrated in the Table 4. Moreover, the binding affinity K_{a1} representing the stronger binding mode was found to be 1 order of magnitude higher (10^7) for the parallel *c-myc* and *c-kit* quadruplexes as compared to antiparallel telomeric quadruplex (10^6). This difference in the binding affinity arises due to the higher association rate constant (k_{a1}) for TMPyP4 binding to parallel *c-myc* and *c-kit* quadruplex as compared to antiparallel telomeric quadruplex (Table 4). However, the dissociation rate constants are found to be same for TMPyP4 interaction with all the three quadruplexes (Table 4). Thus stronger binding has been manifested from the higher association rate constant and not from the lower dissociation rate constant, as no observable change in the k_d values was noticed. Similar dissociation rate constants for both the binding site reveals that occupancy of TMPyP4 in the stronger site does not affect the dissociation rates of TMPyP4 from the second site. This result clearly indicates that the binding sites are independent and do not influence each other. Similar observation was noticed in case of UV studies. It was also observed that ITC isotherms were best fitted with model considering the two independent binding sites. Overall, the data showed that TMPyP4 binds more strongly to parallel *c-myc* and *c-kit* quadruplexes than to the antiparallel telomeric quadruplex, which is in accordance with the UV and ITC data (Tables 2 and 3). Furthermore, the differences obtained in kinetic parameters of TMPyP4 binding to the hairpin duplex and quadruplex were apparent in the plots. TMPyP4 binding to duplex DNA undergoes fast association and dissociation as compared to the quadruplex (Table 4). The larger affinity constants for quadruplex DNA were mainly derived from the effect on dissociation kinetics which is very slow for the quadruplex (Table 4). This observation is well in agreement with results presented by Moore et al. [11] for trisubstituted acridines binding to quadruplex and duplex form of DNA.

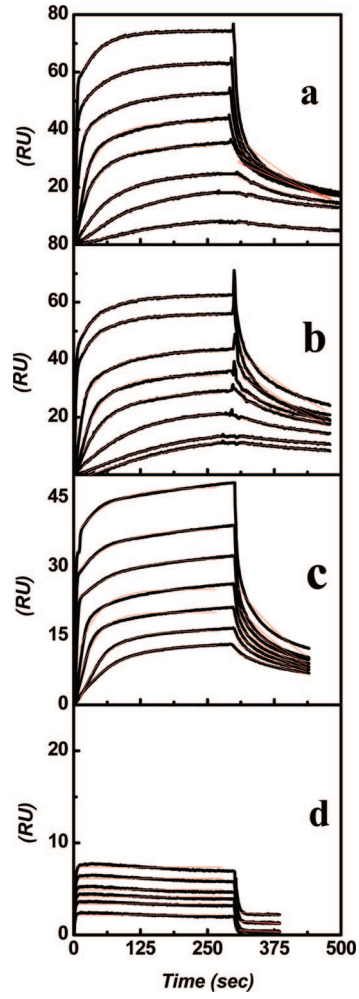

Figure 4. SPR sensorgrams (black) with fitting (red) for the interaction of TMPyP4 with (a) *c-myc,* (b) *c-kit*, (c) telomeric quadruplex, and (d) hairpin duplex DNA (sequences are mentioned in Table 1). The concentration of TMPyP4 increased from 2.5×10^{-8} M (lower curve) to 3.2×10^{-6} M (upper curve).The experiments were conducted in 10 mM HEPES buffer with 100 mM KCl with 0.005% surfactant IGEPAL, pH 7.4, at 25 °C.

Conclusion

The use of small molecules or ligands as therapeutic agents to target G-quadruplexes in the biological system raises concerns about their selectivity and minimum cross reactivity. In this study, all the results (UV, ITC, and SPR) coherently foster that TMPyP4 binds more strongly to the parallel form of the quadruplex than to the antiparallel counterpart. The mode of binding of TMPyP4 to different quadruplexes is also discussed. Among the two binding modes obtained, one is the end stacking mode, wherein the aromatic planar rings of TMPyP4 stack with the end quartet which is accompanied with high binding affinity, whereas the second mode is of external binding, whereby the TMPyP4 molecule interacts with the quadruplex from outside the tetrads stacked externally onto bases at the edges of the loops and is characterized by weak binding interaction. It is inferred that TMPyP4 shows 1 order of magnitude higher binding to quadruplexes as compared to duplex DNA. In all, the study emphasizes that differences in the loop orientation give rise to different conformations of quadruplex, which in turn governs its binding to small molecules and thereby play a pivotal role in their molecular recognition. The thermodynamic parameters obtained would help in a thorough understanding of the ligand−quadruplex interaction, thus providing a platform for designing ligands which could efficiently discriminate one conformation over the other.

Acknowledgment. A.A. acknowledges research fellowship from UGC, INDIA. S.M. acknowledges CSIR for funding this research.

Supporting Information Available: Scatchard plots obtained from UV−vis titration data, representative Scatchard plots obtained from UV−vis reverse titration data, and CD spectra. This material is available free of charge via the Internet at http://pubs.acs.org.

References and Notes

(1) Gellert, M.; Lipsett, M. N.; Davies, D. R. *Proc. Natl. Acad. Sci.U.S.A.* **1962**, *48*, 2013.

(2) Salvati, E.; Leonetti, C.; Rizzo, A.; Scarsella, M.; Mottolese, M.; Galati, R.; Sperduti, I.; Stevens, M. F.; D'Incalci, M.; Blasco, M.; Chiorino, G.; Bauwens, S.; Horard, B.; Gilson, E.; Stoppacciaro, A.; Zupi, G.; Biroccio, A. *J. Clin. Invest.* **2007**, *117*, 3236.

(3) Phatak, P.; Cookson, J. C.; Dai, F.; Smith, V.; Gartenhaus, R. B.; Stevens, M. F.; Burger, A. M. *Br. J. Cancer* **2007**, *96*, 1223.

(4) Rankin, S.; Reszka, A. P.; Huppert, J.; Zloh, M.; Parkinson, G. N.; Todd, A. K.; Ladame, S.; Balasubramanian, S.; Neidle, S. *J. Am. Chem. Soc.* **2005**, *127*, 10854.

(5) Dai, J.; Dexheimer, T. S.; Chen, D.; Carver, M.; Ambrus, A.; Jones, R. A.; Yang, D. *J. Am. Chem. Soc.* **2006**, *128*, 1096.

(6) Cogoi, S.; Xodo, L. E. *Nucleic Acids Res.* **2006**, *34*, 2536.

(7) Khateb, S.; Weisman-Shomer, P.; Hershco-Shani, I.; Ludwig, A. L.; Fry, M. *Nucleic Acids Res.* **2007**, *35*, 5775.

(8) Salas, T. R.; Petruseva, I.; Lavrik, O.; Bourdoncle, A.; Mergny, J. L.; Favre, A.; Saintomé, C. *Nucleic Acid Res.* **2006**, *34*, 4857.

(9) Sharma, S.; Doherty, K. M.; Brosh, R. M., Jr *Curr. Med. Chem. Anticancer Agents* **2005**, *3*, 183.

(10) Martins, C.; Gunaratnam, M.; Stuart, J.; Makwana, V.; Greciano, O.; Reszka, A. P.; Kelland, L. R.; Neidle, S. *Bioorg. Med. Chem. Lett.* **2007**, *17*, 2293.

(11) Moore, M. J.; Schultes, C. M.; Cuesta, J.; Cuenca, F.; Gunaratnam, M.; Tanious, F. A.; Wilson, W. D.; Neidle, S. *J. Med. Chem.* **2006**, *49*, 582.

(12) Casals, J.; Debéthune, L.; Alvarez, K.; Risitano, A.; Fox, K. R.; Grandas, A.; Pedroso, E. *Bioconjug. Chem.* **2006**, *17*, 1351.

(13) Gonçalves, D. P.; Rodriguez, R.; Balasubramanian, S.; Sanders, J. K. *Org. Biomol. Chem.* **2006**, *4*, 3337.

(14) Wei, C.; Jia, G.; Yuan, J.; Feng, Z.; Li, C. *Biochemistry* **2006**, *45*, 6681.

(15) Mita, H.; Ohyama, T.; Tanaka, Y.; Yamamoto, Y. *Biochemistry* **2006**, *45*, 6765.

(16) Han, H.; Langley, D. R.; Rangan, A.; Hurley, L. H. *J. Am. Chem. Soc.* **2001**, *123*, 8902.

(17) Han, F. X.; Wheelhouse, R. T.; Hurley, L. H. *J. Am. Chem. Soc.* **1999**, *121*, 3561.

(18) Anantha, N. V.; Azam, M.; Sheardy, R. D. *Biochemistry* **1998**, *37*, 2709.

(19) Wheelhouse, R. T.; Sun, D.; Han, H.; Han, F. X.; Hurley, L. H. *J. Am. Chem. Soc.* **1998**, *120*, 3261.

(20) Koeppel, F.; Riou, J. F.; Laoui, A.; Mailliet, P.; Arimondo, P. B.; Labit, D.; Petitgenet, O.; Hélène, C.; Mergny, J. L. *Nucleic Acids Res.* **2001**, *29*, 1087.

(21) Rosu, F.; De Pauw, E.; Guittat, L.; Alberti, P.; Lacroix, L.; Mailliet, P.; Riou, J. F.; Mergny, J. L. *Biochemistry* **2003**, *42*, 10361.

(22) Sun, D.; Thompson, B.; Cathers, B. E.; Salazar, M.; Kerwin, S. M.; Trent, J. O.; Jenkins, T. C.; Neidle, S.; Hurley, L. H. *J. Med. Chem.* **1997**, *40*, 2113.

(23) Fedoroff, O. Yu.; Salazar, M.; Han, H.; Chemeris, V. V.; Kerwin, S. M.; Hurley, L. H. *Biochemistry* **1998**, *37*, 12367.

(24) Gomez, D.; Wenner, T.; Brassart, B.; Douarre, C.; O′ Donohue, M. F.; El Khoury, V.; Shin-Ya, K.; Morjani, H.; Trentesaux, C.; Riou, J. F. *J. Biol. Chem.* **2006**, *281*, 38721.

(25) Tauchi, T.; Shin-ya, K.; Sashida, G.; Sumi, M.; Okabe, S.; Ohyashiki, J. H.; Ohyashiki, K. *Oncogene* **2006**, *25*, 5719.

(26) Tahara, H.; Shin-Ya, K.; Seimiya, H.; Yamada, H.; Tsuruo, T.; Ide, T. *Oncogene* **2006**, *25*, 1955.

(27) Binz, N.; Shalaby, T.; Rivera, P.; Shin-ya, K.; Grotzer, M. A. *Eur. J. Cancer* **2005**, *41*, 2873.

(28) Rezler, E. M.; Seenisamy, J.; Bashyam, S.; Kim, M. Y.; White, E.; Wilson, W. D.; Hurley, L. H. *J. Am. Chem. Soc.* **2005**, *127*, 9439.

(29) Gomez, D.; Paterski, R.; Lemarteleur, T.; Shin-Ya, K.; Mergny, J. L.; Riou, J. F. *J. Biol. Chem.* **2004**, *279*, 41487.

(30) Berg, K.; Selbo, P. K.; Weyergang, A.; Dietze, A.; Prasmickaite, L.; Bonsted, A.; Engesaeter, B. O.; Angell-Petersen, E.; Warloe, T.; Frandsen, N.; Høgset, A. *J. Microsc.* **2005**, *218*, 133.

(31) Nyman, E. S.; Hynninen, P. H. *J. Photochem. Photobiol., B* **2004**, *73*, 1.

(32) Han, F. X.; Wheelhouse, R. T.; Hurley, L. H. *J. Am. Chem. Soc.* **1999**, *121*, 3561.

(33) Haq, I.; Trent, J. O.; Chowdhry, B. Z.; Jenkins, C. T. *J. Am. Chem. Soc.* **1999**, *121*, 1768.

(34) Parkinson, G. N.; Ghosh, R.; Neidle, S. *Biochemistry* **2007**, *46*, 2390.

(35) Izbicka, E.; Wheelhouse, R. T.; Raymond, E.; Davidson, K. K.; Lawrence, R. A.; Sun, D.; Windle, B. E.; Hurley, L. H.; Von Hoff, D. D. *Cancer Res.* **1999**, *59*, 639.

(36) Izbicka, E.; Nishioka, D.; Marcell, V.; Raymond, E.; Davidson, K. K.; Lawrence, R. A.; Wheelhouse, R. T.; Hurley, L. H.; Wu, R. S.; Von Hoff, D. D. *Anti-Cancer Drug Des.* **1999**, *14*, 355.

(37) Han, H.; Hurley, L. H.; Salazar, M. *Nucleic Acids Res.* **1999**, *27*, 537.

(38) Sun, D.; Thompson, B.; Cathers, B. E.; Salazar, M.; Kerwin, S. M.; Trent, J. O.; Jenkins, T. C.; Neidle, S.; Hurley, L. H. *J. Med. Chem.* **1997**, *40*, 2113.

(39) Arthanari, H.; Basu, S.; Kawano, T. L.; Bolton, P. H. *Nucleic Acids Res.* **1998**, *26*, 3724.

(40) Li, Y.; Geyer, R.; Sen, D. *Biochemistry* **1996**, *35*, 6911.

(41) Hurley, L. H.; Von Hoff, D. D.; Siddiqui-Jain, A.; Yang, D. *Semin Oncol.* **2006**, *33*, 498.

(42) Huppert, J. L.; Balasubramanian, S. *Nucleic Acids Res.* **2005**, *33*, 2908.

(43) Pasternack, R. F.; Gibbs, E. J.; Villaffranca, *Biochemistry* **1983**, *22*, 2406.

(44) Chaires, J. B. *Methods Enzymol.* **2001**, *340*, 3.

(45) Cantor, C. R.; Schimmel, P. R. *Biophysical Chemistry*; W. H. Freeman: San Fransisco, CA, 1980; Vol 2.

(46) McGhee, J. D.; von Hippel, P. H. *J. Mol. Biol.* **1974**, *86*, 469.

(47) Ghazaryan, A. A.; Dalyan, Y. B.; Haroutiunian, S. G.; Tikhomirova, A.; Taulier, N.; Wells, J. W.; Chalikian, T. V. *J. Am. Chem. Soc.* **2006**, *128*, 1914.

(48) Phan, A. T.; Kuryavyi, V.; Gaw, H. Y.; Patel, D. J. *Nat. Chem. Biol.* **2005**, *1*, 167.

(49) Ambrus, A.; Chen, D.; Dai, J.; Jones, R. A.; Yang, D. *Biochemistry* **2005**, *44*, 2048.

(50) Phan, A. T.; Modi, Y. S.; Patel, D. J. *J. Am. Chem. Soc.* **2004**, *126*, 8710.

(51) Phan, A. T.; Kuryavyi, V.; Burge, S.; Neidle, S.; Patel, D. J. *J. Am. Chem. Soc.* **2007**, *129*, 4386.

(52) Wang, Y.; Patel, D. J. *Structure* **1993**, *1*, 263.

(53) Ambrus, A.; Chen, D.; Dai, J.; Bialis, T.; Jones, R. A.; Yang, D. *Nucleic Acids Res.* **2006**, *34*, 2723.

(54) Qi, J.; Shafer, R. H. *Nucleic Acids Res.* **2005**, *33*, 3185.

(55) He, Y.; Neumann, R. D.; Panyutin, I. G. *Nucleic Acids Res.* **2004**, *32*, 5359.

(56) McElligott, R.; Wellinger, R. J. *EMBO J.* **1997**, *16*, 3705.

JP711608Y